Indonesian Journal of Electrical Engineering and Computer Science
Vol. 29, No. 1, January 2023, pp. 161~173
ISSN: 2502-4752, DOI: 10.11591/ijeecs.v29.i1.pp161-173

Near-field microwave focusing evaluation of dielectric lens antenna for human body model

Amirah Abd Rahman[1], Kamilia Kamardin[1,2], Yoshihide Yamada[1], Masaharu Takahashi[3]
[1]Department of Electronic Systems Engineering, Malaysia-Japan International Institute of Technology, Universiti Teknologi Malaysia, Kuala Lumpur, Malaysia
[2]Wireless Communication Centre, Universiti Teknologi Malaysia, Kuala Lumpur, Malaysia
[3]Center for Frontier Medical Engineering, Chiba University, Chiba, Japan

Article Info

Article history:

Received Jul 27, 2022
Revised Sep 6, 2022
Accepted Sep 28, 2022

Keywords:

Focusing
Hyperthermia
Lenses
Microwave antennas
Noninvasive treatment

ABSTRACT

Various small focus spot applicators are being investigated for hyperthermia therapy, which requires microwave concentration to heat tumors in the human body. Dielectric lens antenna is frequency independent and has strong focusing capability to achieve a very small focusing spot. In this paper, lenses with diameters of 30, 50 and 70 cm were designed to evaluate the size of the focal spot in the human body model. The electromagnetic simulator, FEKO was used to generate rays and near-field focusing data of dielectric lenses at a frequency of 2.45 GHz. The simulated focal spot sizes agreed well with the theoretical values. An analytical investigation into the power at the focal spot was conducted using the proposed power relations of the focused lens novel equation. The theoretical propagation loss is used to represent the power density degradation at the focal spot caused by microwave absorption by the human body. The simulation results of the focused lens in the human body indicated that the 30 cm lens achieved a larger focal spot with a greater focusing power, 0.714 mW compared to the 70 cm lens, which achieved a smaller focal spot but a lower focusing power, which was 0.393 mW.

Corresponding Author:

Kamilia Kamardin
Department of Electronic Systems Engineering, Malaysia-Japan International Institute of Technology
Universiti Teknologi Malaysia
Kuala Lumpur, Malaysia
Email: kamilia@utm.my

1. INTRODUCTION

The use of concentrated microwave radiation to heat tumors has attracted the interest of researchers in employing external microwave applicators on human biological tissues for medical therapy, known as hyperthermia [1], [2]. External microwave hyperthermia is a noninvasive therapy in which the applicator is placed externally near to the targeted tumor [3]. Considering tumors have slower rates of temperature cooling due to restricted blood flow [4], the microwave radiation aims to deliver the power to the tumors to achieve sufficient tumor damage without harming the surrounding healthy tissues. The near-field focused antenna is greatly known for its capability to concentrate radiated electromagnetic (EM) waves to a small focusing spot [5], which is useful for medical treatments that need high-power density at a focal point close to the antenna aperture.

In the case of focused hyperthermia applicator, several types of antennas [6]-[12] were designed to localize microwave power in human biological tissues. Initially, the adaptive phased array hyperthermia system was designed [13] to produce the required field intensity at the tumor and eliminate unintended hot spots. Multiple antennas phased array systems with rigid antenna components were also developed [14], [15] and have been used in clinical trials to treat head and neck targets [16]. Although these applicators provide advanced energy deposition control, system complexity, as well as large dimensions and weight, must be addressed in a clinical setting. In addition, more research was conducted to obtain small focusing spot to ensure localization of microwave power to the targeted tumor tissue. A near-field focused folded transmit array antenna [17] with a diameter of D=54 cm was positioned 40 cm in front of human leg tissues for medical applications. The focusing spot had a radius of 7.5 cm at -3dB spot area. Another 2.4 GHz near-field 4×4 microstrip focused array antenna for medical applications was also presented [18]. According to the simulation, a −3dB spot was enclosed in a region of approximately 10 cm, that has been mentioned to be adequate for focusing the EM power in small areas of biological tissues for clinical application. However, the operating frequency band of array antenna was limited. A 19 cm cylindrical left-handed metamaterial (LHM) lens to heat superficial tumor at 2.45 GHz was proposed [19]. Depending on the distance between two microwave sources, the achieved focused resolution ranged from 0.7 to 2.04 cm. Nonetheless, the metamaterial-based antennas have certain limitations, such as the fact that it only operates in a restricted frequency range and is difficult to manufacture.

The novelty of this paper is that it evaluates the near-field focusing of the fundamental dielectric lens antenna that concentrates microwave into the human body model relative to the antenna diameter. Although the proposed focused lens design is unable to represent real condition of the hyperthermia therapy applicator, it is somehow useful to investigate the condition of power concentration and the focal spot size inside the human body model which provides significant information for designing hyperthermia therapy applicators in the future.

The paper is organized as shown in; section 2 introduces the fundamental design concept of the focused dielectric lens antenna, theoretical concept of the followings; focal spot size, power relations of the lens and power degradation in the lossy material. The simulation parameters of the focused dielectric lens are then provided in section 3. In Section 4, the simulations results of the electric power concentration at the focus spot are presented. Section 5 concludes the findings obtained from the analysis in the paper.

2. FOCUSED DIELECTRIC LENS ANTENNA DESIGN

The equations to design the lens shapes are explained. The lenses were designed for the free space and the human body model. The lens shaping accuracy was validated using the ray tracing method based on ray launching-geometrical optics (RL-GO).

2.1. Fundamental of the dual focused lens antenna

In the first convex lens, the distance from the feed to the first hyperbolic lens surface, S_1 is expressed by r_1. Flat surface of the first convex lens is S_2 while its central thickness is T_1. Another hyperbolic surface for the second convex lens is indicated by S_4. The ray path from S_4 to the Focus 2 is represented by r_2. The flat surface for second convex lens is S_3 and its central thickness is T_2. Around the z-axis, the lens is rotated symmetrically, and the radial direction of the lens corresponds to the y-axis as shown in Figure 1.

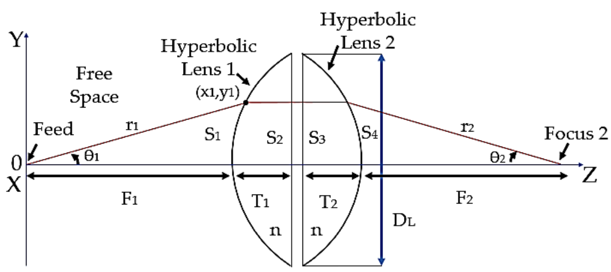

Figure 1. Dual focused lens structure

The feed was set at the coordinates of (0,0). The hyperbolic surfaces of lens 1 (i=1) and lens 2 (i=2) were determined by (1) [20]. The focal length is defined by F and the refractive index is defined by n.

$$r_i = \frac{(n-1)F_i}{n\cos\theta_i - 1} \tag{1}$$

The ray path, r begins at the feed point and ends at the Focus 2 point. The lens thickness, T_i [20] is given by (2) with D_L denoting the lens diameter.

$$T_i = \frac{1}{n+1}\left(\sqrt{F_i^{\,2} + \frac{(n+1){D_L}^2}{4(n-1)}} - F_i\right) \quad (2)$$

The feed emits a spherical wave at (0,0) coordinates, transforms to a plane wave when passing through the converging lens, and then returns to a spherical wave at Focus 2.

2.2. Ray tracing of the focused dielectric lens antenna in the free space

Lens antenna shaping accuracy is validated using the ray launching-geometrical optics (RL-GO) solver of the FEKO simulator. The rays are shown in Figure 2. Ray tracing result shows that the lens shape was correctly designed as the focal length F_1 equals F_2. The simulation parameters of the ray analysis in Figure 2 are shown in Table 1.

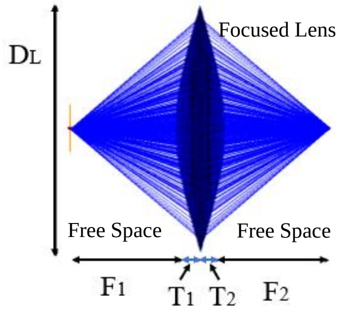

Figure 2. Ray analysis of focused dielectric lens D_L=30 cm

Table 1. Focused dielectric lens antenna configuration in free space

Parameter	Value
Refractive Index (n)	3
Lens Diameter (D_L)	30 cm
Focal Length ($F_1 = F_2$)	13 cm
Lens Thickness ($T_1 = T_2$)	2.97 cm

2.3. Focused dielectric lens antenna to focus inside the human body model

Focused lens structure for human body model is shown in Figure 3. The human body part is shown by the area with refractive index n_2 (n_2>n_1). The focus point is indicated by focus 2.

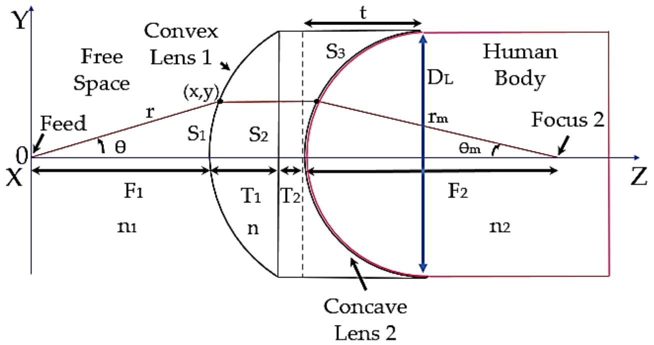

Figure 3. Focused lens structure for human body model

The concave lens shape to focus EM waves in the human body equivalent tissue model was designed by modifying (1) into (3):

$$r_m = \frac{F_2(n_2 - n)}{(n_2 - n\cos\theta_m)} \quad (3)$$

The refractive index of the human body, n_2 takes the value of $n_2 = \sqrt{(<\varepsilon_r>)}$, where ε_r is defined as (4).

$$< \varepsilon_r > = \varepsilon_r - j\frac{\sigma}{\omega\varepsilon_0} = \varepsilon_r - j60\lambda_0\sigma \quad (4)$$

In the case of actual human tissues, conductivity ranges from $0.1<\sigma<2$ [21]. In most cases, $\sigma<0.5$ is dominant. In this paper, $\sigma=0.5$ was applied to (4). Therefore, $<\varepsilon_r>=52.7–j3.6$. For the convenience of calculation, ε_r takes the value of 52.7 while σ can be neglected. Ray, r of the convex lens was designed by using (1) and T_1 of the convex lens was determined using (2). Then, convex and concave lenses were combined using (5).

$$r.\sin\theta = r_m.\sin\theta_m = \frac{D_L}{2} \quad (5)$$

As the thickness of concave lens, T_2 was set to a predetermined value, t was calculated and can be obtained using (6).

$$t = F_2 - \cos\theta_m \cdot r_m \quad (6)$$

2.4. Ray tracing of the the focused dielectric lens antenna for the human body model

The focused dielectric lens antenna for the human body model was analysed using RL-GO solver. The simulation involved three different mediums: free space, lens and human body of refractive index, $n_1=1$, $n=3$ and $n_2=7.26$, respectively. The produced rays as in Figure 4 clearly verified that the focused dielectric lens antenna concept for human body was designed according to the derived equations. The characteristics of the focused dielectric lens antenna for the human body are shown in Table 2.

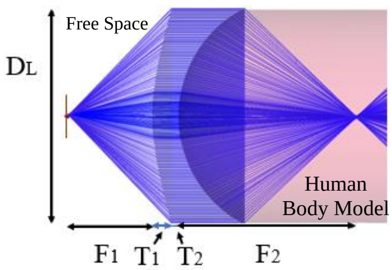

Figure 4. Ray analysis of focused dielectric lens antenna for the human body model

Table 2. Focused dielectric lens antenna configuration for the human body

Parameter	Value
Refractive Index (n)	3
Lens Diameter (D_L)	30 cm
Focal Length (F_1)	13 cm
Focal Length (F_2)	26.1 cm
Lens Thickness (T_1)	2.97 cm
Lens Thickness (T_2)	1 cm

2.5. Theoretical focal spot size

Focusing antenna concentrates microwave energy at a point in front of the lens in a small spot. As a result, energy is focused in one direction and energy transmission in other directions are avoided [22]. Theoretical focal spot size, S_T of lens antenna [23] can be calculated using (7). The wavelength in a medium is indicated by λ_g. While, F_{Total} equals to the summation of the focal length and half of the converging lens' thickness.

$$S_T = \frac{1.22F_{Total}\lambda_g}{D_L} \quad (7)$$

According to the expression d in Figure 5, its relation to the spot size is described by (8):

$$d = 2S_T \tag{8}$$

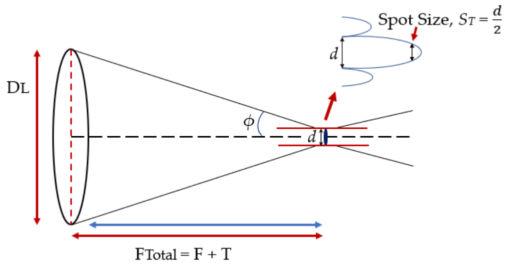

Figure 5. Focal spot size parameters of focused lens antenna

2.6. Power relations of the focused dielectric lens

Equations that express power relations of the lens were derived according to the diagram shown in Figure 6. The captured power inside the cone area of θ_L (rad), P_C is expressed by (9) with A_C as the captured area and the transmitted power of the feed dipole antenna is represented by P_T.

$$P_C = \frac{A_C}{4\pi r^2} P_T \tag{9}$$

The captured area, A_C of the lens area can be calculated by (10).

$$A_C = \pi {\theta_L}^2 r^2 \tag{10}$$

Angle, θ_L (rad) is calculated by (11).

$$\theta_L = tan^{-1} \frac{(D_L/2)}{F+t} \; [rad] \tag{11}$$

Then, P_C is expressed by (12).

$$P_C = \frac{{\theta_L}^2}{4} P_T \tag{12}$$

The following expressions (13)-(15) were considered to calculate the transmission coefficient, T_1 and T_2 and the power transmitted by lens antenna, P_L.

$$T_1 = \frac{4n_1n_2}{(n_1+n_2)^2} \tag{13}$$

$$T_2 = \frac{4n_2n_3}{(n_2+n_3)^2} \tag{14}$$

$$P_L = P_C T_1 T_2 = \frac{{\theta_L}^2}{4} P_T T_1 T_2 \tag{15}$$

The area of the focal spot, A_S is indicated by (16) with S is the diameter of the focal spot size. The power, P_{-3} at -3dB power density, W_{-3} is given by (17).

$$A_S = \pi \left(\frac{S}{2}\right)^2 \tag{16}$$

$$P_{-3} = A_S W_{-3} \tag{17}$$

Then, the concentrated power at the focal spot, P_S is given by (18).

$$P_S = 1.5 P_{-3} \tag{18}$$

The diagram in Figure 6 describes the focal spot power, P_S, the outside power that surrounded the spot area, P_O and the diffracted power, P_D as the three components of the lens antenna power, P_L. P_D is produced by multiple reflections inside the lens.

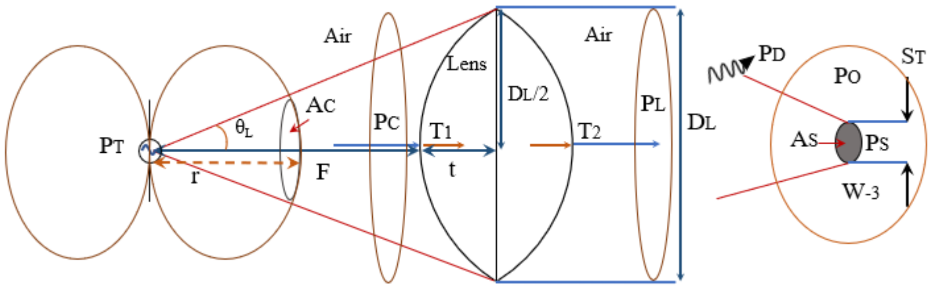

Figure 6. Power transmission through lens

2.7. Power degradation in the lossy material

In EM waves propagation, electric field (E-field) in the lossy material is expressed as follows (19). Where σ indicates the conductivity of the material and α is the attenuation constant (20) in nepers per meter (Np/m). The EM waves travelling distance is denoted by z which is in meter (m).

$$E(z) = E_o e^{-\alpha z} \tag{19}$$

$$\alpha = \omega \sqrt{\frac{\mu_0 \varepsilon_0 \varepsilon_r}{2} \left[\sqrt{1 + \left(\frac{\sigma}{\omega \varepsilon_0 \varepsilon_r} \right)^2} - 1 \right]} \tag{20}$$

In addition, the propagation loss, P_{Loss} in the lossy material given by (21) was used to estimate the power degradation within the human body model when EM waves is focused by the lens.

$$P_{Loss}(dB) = 20\,log\, e^{-\alpha z} = -\,8.686\alpha z \tag{21}$$

3. SIMULATION BY THE ELECTROMAGNETIC SIMULATOR

The simulation of the focused lens design in the free space and for the human body model were investigated using lenses with diameters, D_L of 30, 50, and 70 cm at 2.45 GHz. The simulation by the electromagnetic simulator, FEKO were performed to interpolate the focal spot sizes ranging from 30 to 70 cm. The simulation parameters are presented in Table 3.

Table 3. Simulation parameters for the focused dielectric lens antenna

Item	Parameter	Value		
EM Simulator Solver	-	FEKO 2019, MoM/ FEM Hybrid		
Frequency (f)	-	2.45 GHz		
Wavelength (λ_0)	-	12.24 cm		
Feed Antenna (Half- λ Dipole)	Length	5.836 cm		
	Wire Radius	0.01224 cm		
	Transmit Power (P_T)	0.014 W [R_{in}=73 Ω, V= 1V]		
Lens 1	Refractive Index (n)	3		
(Lens 2 in Free Space)	Diameter (D_L)	30 cm	50 cm	70 cm
	Focal Length (F_1= F_2)	13 cm	15 cm	20 cm
	Wavelength (λ)	12.24 cm		
Lens 2 for Human Body	Refractive Index (n)	3		
	Diameter (D_L)	30 cm	50 cm	70 cm
	Focal Length (F_1)	13 cm	15 cm	20 cm
	Focal Length (F_2)	26.1 cm	40.8 cm	56.8 cm
Human Body	Permittivity (ε_r)	52.7		
	Conductivity (σ)	0 (Spot size calculation) 0, 0.5, 1.0 & 1.95 (Power degradation)		
	Wavelength (λ_g)	1.69 cm		

Simulation models for investigating the focal spot size using focused lens Figure 7. The simulation model of the focused lens in the free space is shown in Figure 7(a), whereas Figure 7(b) depicts the simulation model of a human body. Close proximity configuration can improve microwave energy coupling and localization to the tissue. Therefore, the simulation for the human body condition is regarded as the simulation purpose only and does not portray the real human body condition because the initial simulation data needs to be collected and analyzed.

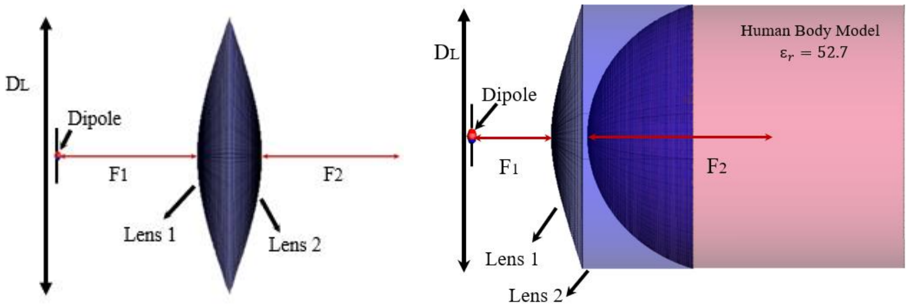

Figure 7. Simulation models for investigating the focal spot size using focused lens; (a) focused lens in the free space and (b) focused lens for the human body model

Simulated performance of the feed antenna Figure 8. The simulation model of the focused dielectric lens antenna in the free space was used to verify the lens focusing concept while, the focused dielectric lens antenna for the human body was used to investigate the focal spot size and electric power distributions in a human body model. Half- wavelength dipole antenna was used as the feed antenna due to its simplicity. The simulated performance of the feed antenna in terms of radiation pattern and normalized reflection coefficient, S_{11} are illustrated in Figures 8(a) and 8(b), respectively. The radiation pattern shows that the power was distributed omni-directionally over a radiation sphere.

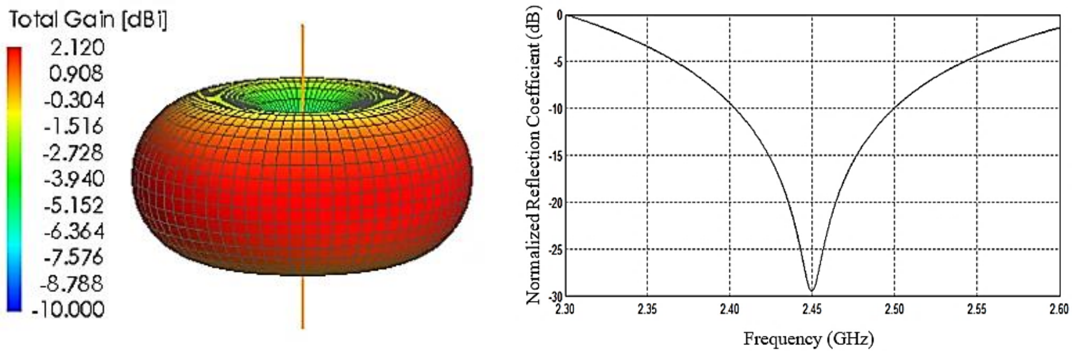

Figure 8. Simulated performance of the feed antenna based on (a) radiation pattern and (b) S_{11}

4. ELECTRIC POWER CONCENTRATION AT THE FOCUS SPOT

In order to ensure the focusing ability of the focused lens, focusing analysis at the focus spot in the free space is first presented in terms of the focal spot size evaluation. Then, the power concentration at the focus spot is described. The same approach is applied to evaluate the focusing performance inside the human body model.

4.1. Focusing of power in the free space

The results of the free space focusing conditions are shown in Table 4. Power is concentrated around $Z=F_2$ in the Y-Z plane and power is distributed along the Z axis. The power concentration spot becomes small with a large lens diameter. The spot sizes at -3dB are represented by the power distributions in the X-Y plane.

Table 4. Simulated power density distribution in the free space

D_L (cm)	Power Density (dBW/m^2) Y-Z plane	Power Density (dBW/m^2) X-Y plane at $Z = F_2$
30	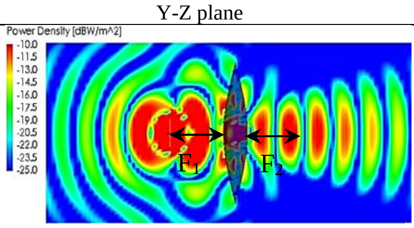	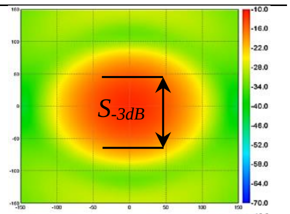
50	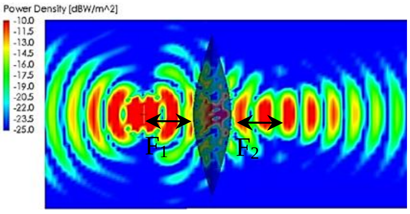	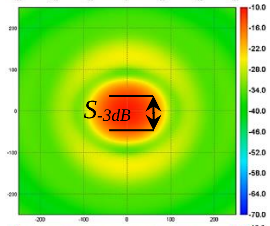
70	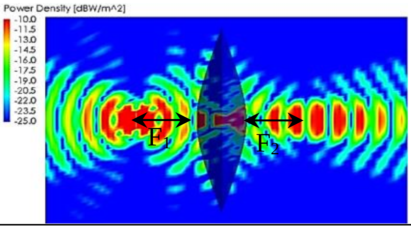	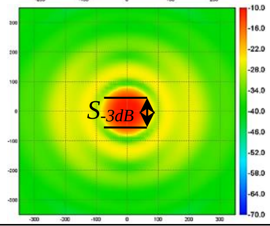

Simulated near-fied focusing in the free space for DL=30, 50 and 70 cm in terms of as shown in Figure 9. The near-field focusing effects in the free space in terms of the focal spot size and the power densities are shown in Figures 9(a) and (b), respectively. The theoretical spot size, S_T of (7) are compared to the simulated focal spot size, S_{-3dB} in Figure 9(a). Although S_{-3dB} values are larger than S_T, the trend of both S_{-3dB} and S_T values shows good agreement for all cases of D_L=30, 50 and 70 cm.

However, evaluation of the focal spot size in the free space is not significant in this study; nonetheless, it demonstrates that the approach can be utilized to validate the focal spot size in the human body model. The simulated power density values at the focal spot for D_L=30, 50 and 70 cm are shown in Figure 9(b). The increase in power density is approximately proportional to the increment of the lens antenna diameter, D_L.

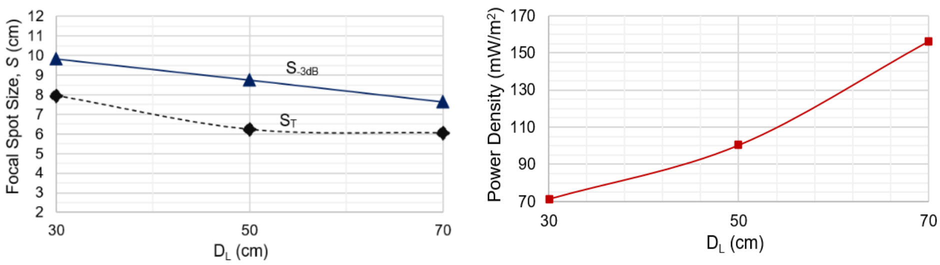

(a) (b)

Figure 9. Simulated near-fied focusing in the free space for D_L=30, 50 and 70 cm in terms of (a) focal spot size and (b) power densities

4.2. Power at the focus spot in the free space

In order to evaluate the power concentration at the focus spot that is produced by the focused dielectric lens antenna, calculations were performed according to (9)-(18). Following that, the calculated power values are summarized in Table 5. The transmit power source, P_T by the feed antenna was calculated using (22).

$$P_T = \frac{V^2}{R} = \frac{1^2}{73}\,(\text{W}) \quad (22)$$

Table 5. Power relations in the free space

D_L (cm)	P_T (W)	θ_L (rad)	P_C (mW)	T_1T_2	P_L (mW)	W_{-3} (mW/cm^2)	A_S (cm^2)	P_{-3} (mW)	P_S (mW)
30	0.014	0.754	1.99	0.56	1.12	0.00359	76.05	0.273	0.409
50	0.014	0.876	2.69	0.56	1.51	0.00507	60.27	0.306	0.458
70	0.014	0.890	2.77	0.56	1.56	0.00779	45.84	0.357	0.536

The estimated values of P_S which is $P_S=P_L/3$ denotes that $P_D=P_O=P_S$. As described previously in section 2.6, P_L is composed of P_S, P_O and P_D. Power relation between P_L and power at focal spot, P_S is shown in Figure 10 which is reduced to only one third of the power that is produced by the focused dielectric lens antenna.

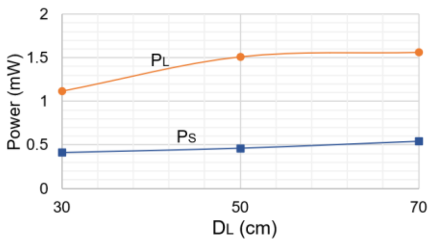

Figure 10. Power relations in the free space

4.3. Focusing of power inside the human body model

In the focused hyperthermia therapy, radiation deposition into the human biological tissues is preferred to be in minimum spot size which indicates that only the area at the focal point will be heated rather than the surrounding areas. The simulated power densities at the focal spot within the human body model are shown in Table 6. Data at σ=0 were used to analyse the spot sizes. As the conductivity inside the human body model increased, power density at the focal point decreased. Moreover, the focal spot size decreased with increasing lens diameter. As shown in Table 6, power density degradation was significantly greater at σ=1.0 for D_L=50 cm.

Simulated near-fied focusing inside the human body for DL=30, 50 and 70 cm in terms of as shown in Figure 11. The near-field focusing effects inside the human body in terms of the focal spot size and the power densities are shown in Figure 11(a) and (b), respectively. The spot sizes obtained from the simulations in the X-Y plane at $Z=F_2$ are plotted in Figure 11(a). The S_T and S_{-3dB} in the human body matched extremely well. The size of the focal spots in the human body model appeared to be smaller due to the higher relative permittivity, ε_r of the human body [24] compared to the free space. As shown in Figure 11(b), the simulated power densities at the focal spot for σ=0 increased as D_L increased.

4.4. Power at the focus spot inside the human body model

Subsequently, the total power concentrated at the spot area in the human body model was calculated. The calculated values using (9)-(18) were based on the calculation of the free space condition. The calculated values are summarized in Table 7.

As described in Figure 12, power that was produced by the lens antenna, P_L was higher in D_L=70 cm as compared to D_L=30 cm. However, the P_S of D_L=70 cm was lower than the Ps of D_L=30 cm. Referring to Table 7, $P_S= P_L/2$ for D_L=30 cm. Meanwhile, $P_S=P_L/4$ for D_L=70 cm. The lower value of Ps for D_L=70 cm is due to the lower P_{-3} value in which, according to (17), having a smaller focal spot area, A_S has resulted in a lower P_{-3} value. This is true in the case of D_L=70 cm because a smaller focal spot size was achieved by D_L=70 cm as compared to D_L=30 cm. This is also supported by the slight variation in -3 dB power density, W_{-3} between D_L=30, 50 and 70 cm. In addition, the P_O of D_L=70 cm was greater than the P_O of D_L=30 cm.

At 2.45 GHz, a human body equivalent tissue model with relative permittivity of 52.7 and conductivity of 1.95 was referred [25] to investigate power density at the focal spot that is influenced by the conductivity of the human body. A lens of D_L=50 cm was used in the simulation with human body conductivity values of 0, 0.5, 1.0 and 1.95. Table 8 displays the variation in power densities as a function of conductivity and the P_{Loss} values calculated. The P_{Loss} were calculated using (21) with the microwave traveling distance, z=40.8 cm or 0.408 m that equals to F_2 in the human body model. It was demonstrated that, considering the impact of conductivity in the human body, the obtained P_{Loss} values may be utilized to determine the power density degradations at the focusing spot.

Table 6. Simulated power density distribution inside the human body

D_L (cm)	σ	Power Density (dBW/m^2) Y-Z plane	Power Density (dBW/m^2) X-Y plane Z = F_2
30	0	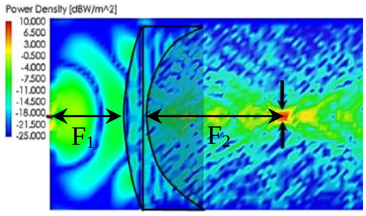	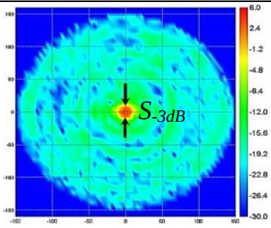
50	0	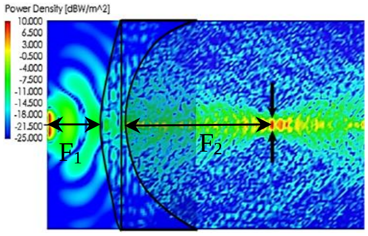	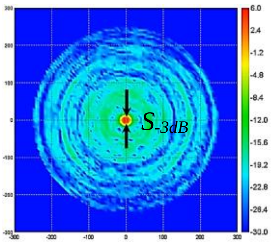
50	1.0	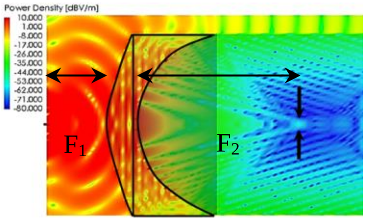	
70	0	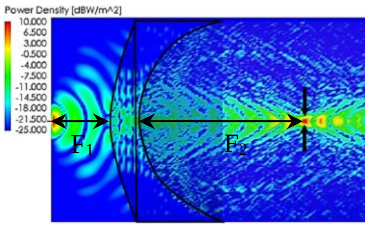	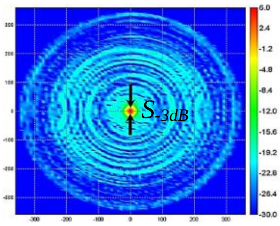

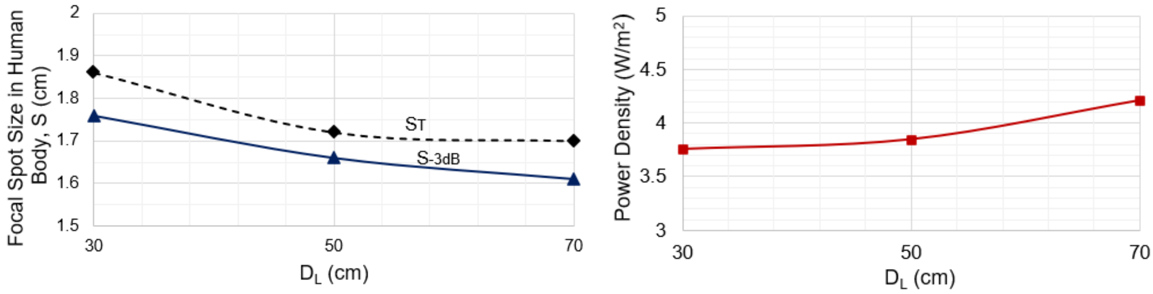

(a) (b)

Figure 11. Simulated near-fied focusing inside the human body for D_L=30, 50 and 70 cm in terms of (a) focal spot size and (b) power densities of σ=0

Table 7. Power relations in the human body model

D_L (cm)	P_T (W)	θ_L (rad)	P_C (mW)	T_1T_2	P_L (mW)	W_{-3} (mW/cm^2)	A_S (cm^2)	P_{-3} (mW)	P_S (mW)
30	0.014	0.754	1.99	0.62	1.24	0.196	2.43	0.476	0.714
50	0.014	0.876	2.69	0.62	1.67	0.210	1.86	0.390	0.585
70	0.014	0.890	2.77	0.62	1.73	0.228	1.15	0.262	0.393

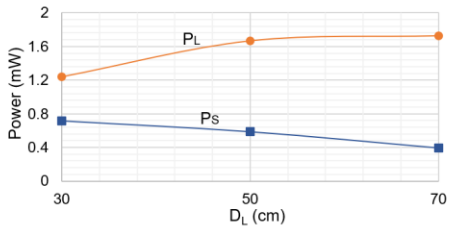

Figure 12. Power relation in the human body model

Table 8. Variation in power densities and the estimation of power degradations of D_L=50 cm

ε_r	σ	α	Power Density (dBW/m^2)	Normalized Power Density (dBW/m^2)	P_{LOSS} (dB) *(21)
52.7	0	0	5.51	0	0
	0.5	13	- 36.9	- 42.41	- 46.07
	1.0	26	- 78.6	- 84.11	- 92.14
	1.95	50	- 147.0	- 152.51	- 177.19

5. CONCLUSION

In this paper, the focusing ability of the dielectric lens antenna to achieve a small spot size in the human body model were verified through the construction of lenses with diameters of 30, 50 and 70 cm at 2.45 GHz. The simulation results shows that the power density at the focal spot were reduced due to the increased conductivity of the human body model. In addition, the power density degradation at the focal spot in the human body model due to the conductivity can be estimated using the P_{Loss} equation. Through the theoretical analysis of power estimation at the focal spot, it was shown that the focused dielectric lens antenna of D_L = 30 cm achieved higher focusing power compared to the D_L=0 cm. Despite the fact that the lenses in this study were not tested in the experiment due to their large diameter, the simulation results demonstrated that the proposed theoretical equations are valid. The findings in this paper contributed to an understanding of the approach to achieve a small focal spot size in the human body and the power degradation condition, which could be used as a guide for designing, fabricating, and testing smaller and thinner focused dielectric lens antenna for hyperthermia therapy in the near future.

ACKNOWLEDGEMENTS

Authors would like to thank the Ministry of Higher Education, Malaysia for the research grants (research grant numbers 16J46 and 5F063) and Ministry of Health, Malaysia for the HLP scholarship. This research is also supported by Japan International Cooperation Agency (JICA) through JICA Joint Research Grant 2021.

REFERENCES

[1] M. H. Seegenschmiedt and C. C. Vernon, *A historical perspective on hyperthermia in oncology*. Berlin, Heidelberg: Springer, 1995.
[2] M. I. Priester, S. Curto, G. C. van Rhoon, and T. L. M. Ten Hagen, "External basic hyperthermia devices for preclinical studies in small animals," *Cancers*, vol. 13, no. 18, p. 4628, Sep. 2021, doi: 10.3390/cancers13184628.
[3] H. P. Kok *et al.*, "Heating technology for malignant tumors: a review," *International Journal of Hyperthermia*, vol. 37, no. 1, pp. 711–741, Jan. 2020, doi: 10.1080/02656736.2020.1779357.
[4] K. Shchors and G. Evan, "Tumor angiogenesis: Cause or consequence of cancer?," *Cancer Research*, vol. 67, no. 15, pp. 7059–7061, Aug. 2007, doi: 10.1158/0008-5472.CAN-07-2053.
[5] P. Nepa and A. Buffi, "Near-field-focused microwave antennas: Near-field shaping and implementation," *IEEE Antennas and Propagation Magazine*, vol. 59, no. 3, pp. 42–53, Jun. 2017, doi: 10.1109/MAP.2017.2686118.
[6] R. Sen, T. D. Jerome-Surendran, D. K. Trivedi, M. A. Qayyum, and B. P. Kumar, "Generalised method of current excitation reconstruction from near-field data of planar, cylindrical and spherical antenna arrays," *IET Microwaves, Antennas and Propagation*, vol. 7, no. 14, pp. 1128–1136, Nov. 2013, doi: 10.1049/iet-map.2012.0208.
[7] W. C. Choi, S. Lim, and Y. J. Yoon, "Design of noninvasive hyperthermia system using transmit-array lens antenna configuration," *IEEE Antennas and Wireless Propagation Letters*, vol. 15, pp. 857–860, 2016, doi: 10.1109/LAWP.2015.2477428.
[8] M. Krairiksh, T. Wakabayashi, and W. Kiranon, "A spherical slot array applicator for medical applications," *IEEE Transactions on Microwave Theory and Techniques*, vol. 43, no. 1, pp. 78–86, 1995, doi: 10.1109/22.363004.
[9] R. V. Sabariego, L. Landesa, and F. Obelleiro, "Synthesis of an array antenna for hyperthermia applications," *IEEE Transactions on Magnetics*, vol. 36, no. 4 I, pp. 1696–1699, Jul. 2000, doi: 10.1109/20.877769.
[10] R. J. Lalonde, A. Worthington, and J. W. Hunt, "Field conjugate acoustic lenses for ultrasound hyperthermia," *IEEE Transactions on Ultrasonics, Ferroelectrics, and Frequency Control*, vol. 40, no. 5, pp. 592–602, Sep. 1993, doi: 10.1109/58.238113.

[11] E. A. Lekka, K. D. Paschaloudis, and G. A. Kyriacou, "Phased array design for near field focused hyperthermia based on reciprocity theorem," in *2017 International Workshop on Antenna Technology: Small Antennas, Innovative Structures, and Applications, iWAT 2017*, 2017, pp. 277–280, doi: 10.1109/IWAT.2017.7915379.
[12] I. Merunka, O. Fiser, L. Vojackova, J. Vrba, and D. Vrba, "Utilization potential of balanced antipodal Vivaldi antenna for microwave hyperthermia treatment of breast cancer," in *8th European Conference on Antennas and Propagation, EuCAP 2014*, Apr. 2014, pp. 706–710, doi: 10.1109/EuCAP.2014.6901857.
[13] A. J. Fenn and G. A. King, "Adaptive radiofrequency hyperthermia-phased array system for improved cancer therapy: Phantom target measurements," *International Journal of Hyperthermia*, vol. 10, no. 2, pp. 189–208, Jan. 1994, doi: 10.3109/02656739409009343.
[14] J. Stang, M. Haynes, P. Carson, and M. Moghaddam, "A preclinical system prototype for focused microwave thermal therapy of the breast," *IEEE Transactions on Biomedical Engineering*, vol. 59, no. 9, pp. 2431–2438, Sep. 2012, doi: 10.1109/TBME.2012.2199492.
[15] L. Wu, R. J. McGough, O. A. Arabe, and T. V. Samulski, "An RF phased array applicator designed for hyperthermia breast cancer treatments," *Physics in Medicine and Biology*, vol. 51, no. 1, pp. 1–20, Jan. 2006, doi: 10.1088/0031-9155/51/1/001.
[16] M. M. Paulides, J. F. Bakker, N. Chavannes, and G. C. Van Rhoon, "A patch antenna design for application in a phased-array head and neck hyperthermia applicator," *IEEE Transactions on Biomedical Engineering*, vol. 54, no. 11, pp. 2057–2063, Nov. 2007, doi: 10.1109/TBME.2007.895111.
[17] S. H. Zainud-Deen, W. M. Hassan, and H. A. Malhat, "Near-field focused folded transmitarray antenna for medical applications," *Wireless Personal Communications*, vol. 96, no. 3, pp. 4885–4894, Oct. 2017, doi: 10.1007/s11277-017-4433-7.
[18] F. Tofigh, J. Nourinia, M. Azarmanesh, and K. M. Khazaei, "Near-field focused array microstrip planar antenna for medical applications," *IEEE Antennas and Wireless Propagation Letters*, vol. 13, pp. 951–954, 2014, doi: 10.1109/LAWP.2014.2322111.
[19] Y. Tao and G. Wang, "A new hyperthermia scheme with a cylindrical LHM Lens," *APCBEE Procedia*, vol. 7, pp. 32–36, 2013, doi: 10.1016/j.apcbee.2013.08.008.
[20] Y. T. Lo and S. W. Lee, *Antenna Handbook Volume I-IV*, no. Bd. 1. Van Nostrand Reinhold Company, 1993.
[21] C. Gabriel, "Compilation of the Dielectric properties of body tissues at RF and microwave frequencies.," 1996. doi: Report N.AL/OE-TR- 1996-0037.
[22] J. Thornton and K. C. Huang, *Modern Lens Antennas for Communications Engineering*. Hoboken, NJ, USA: John Wiley & Sons, Inc., 2013.
[23] G. R. Fowles and D. W. Lynch, "Introduction to modern optics," *American Journal of Physics*, vol. 36, no. 8, pp. 770–771, Aug. 1968, doi: 10.1119/1.1975142.
[24] S. Altunc, C. Baum, C. Buchenauer, C. Christodoulou, and E. Schamiloglu, "Design of a special dielectric lens for concentrating a subnanosecond electromagnetic pulse on a biological target," *IEEE Transactions on Dielectrics and Electrical Insulation*, vol. 16, no. 5, pp. 1364–1375, Oct. 2009, doi: 10.1109/TDEI.2009.5293950.
[25] C. J. Robert F., D. M. Sylvar, and J. L. Ulcek, "Evaluating compliance with FCC guidelines for human exposure to radiofrequency electromagnetic fields," *FCC OET Bulletin 65*, no. August, pp. 1–79, 1997.

BIOGRAPHIES OF AUTHORS

Ir. Amirah Abd Rahman received Bachelor of Engineering (Hons.) Electronics from the Multimedia University, Malaysia and Master of Engineering (Biomedical Engineering) from the University of Malaya, Malaysia. She serves as an electronic engineer at Ministry of Health, Malaysia. She is currently a Ph. D student in engineering (applied electromagnetics) at the University of Technology Malaysia. She is a Professional Engineer registered under the Board of Engineers Malaysia (BEM) and a Professional Technologist under the Malaysia Board of Technologist (MBOT). She is a registered ASEAN Chartered Professional Engineer. She can be contacted at email: amirah.ar@graduate.utm.my.

Ir. Dr. Kamilia Kamardin (corresponding author) received B.Eng. Electronic (Communications) from the University of Sheffield, U.K., in 2004 and obtained her M.Sc. in Information Technology (Data Communications and Networking) from Universiti Teknologi Mara (UiTM), Malaysia in 2007. She received her Ph.D. in Electrical Engineering (Communications) from Universiti Teknologi Malaysia (UTM), Malaysia in 2014. She spent 3 months at University of Bimingham, U.K., as a visiting Ph.D. student. She has previously served as a senior assistant researcher at TM Research and Development, Malaysia for 3 years. Currently she serves as a senior lecturer at department of Electronic Systems Engineering, Malaysia-Japan International Institute of Technology (MJIIT), UTM Kuala Lumpur. She is also an associate member of Wireless Communication Centre (WCC). She is an IEEE senior member and hold treasurer position for IEEE Malaysia AP/MTT/EMC joint chapter from 2018 until 2022. She is also a Professional Engineer registered under the Board of Engineers Malaysia (BEM) and a Professional Technologist under the Malaysia Board of Technologist (MBOT). Her research interests include antennas and propagation, body centric communication, wearable communication, metamaterials and Internet of Things (IoT). She can be contacted at email: kamilia@utm.my.

Prof. Dr. Yoshihide Yamada received bachelor (B. Eng) and master (M. Eng) of engineering from Nagoya Institute of Technology, Japan in 1971 and 1973, respectively. And he received the Dr. of electrical engineering (DE) from Tokyo Institute of Technology in 1989. He joined Electrical Communication Laboratories of Nippon Telegraph and Telephone Corporation (NTT) in 1973 and moved to NTT Mobile Communications Network Inc. (NTT DoCoMo) in 1993. In 1998, he joined National Defense Academy as a professor. In 2014, he joined Malaysia-Japan International Institute of Technology (MJIIT) at UTM, Malaysia as a professor. He received the excellent paper award and the tutorial paper award from IEICE in 2013 and 2014, respectively. His research interests are aperture antennas, array antennas, very small antennas and radar cross sections. He is a Fellow of IEICE Japan, senior member of IEEE APS and a member of ACES. He can be contacted at email: yoshihide@utm.my.

Prof. Dr. Masaharu Takahashi received the B.E. degree in electrical engineering in 1989 from Tohoku University, Miyagi, Japan, and the M.E. and D.E. degree in electrical engineering from Tokyo Institute of Technology, Tokyo, Japan, in 1991 and 1994, respectively. He was a Research Associate from 1994 to 1996, an Assistant Professor from 1996 to 2000 at Musashi Institute of Technology, Tokyo, Japan, and an Associate Professor from 2000 to 2004 at Tokyo University of Agriculture & Technology, Tokyo, Japan. He is currently an Associate Professor at Chiba University, Japan. He served as Editor-in-Chief of IEICE Transactions on Communication from 2011 to 2013, Vice Chair of Editorial Board, IEICE Communication Society from 2013 to 2014, Editor in chief of Editorial committee of IEICE Communications Society Magazine (Japanese Edition) from 2014 to 2016, Chair of Technical Committee on Wireless Power Transfer, IEICE from 2018 to 2020, Vice President of IEICE-CS Board from 2019 to 2021, Chair of Planning and Member Activities Committee, IEICE-CS from 2019 to 2021, and Chair of IEEE Antennas & Propagation Society Tokyo Chapter from 2019 to 2020. His main interests have been electrically small antennas, RFID, planar array antennas (RLSA), EMC and research on evaluation of the interaction between electromagnetic fields and the human body by use of numerical and experimental phantoms. He received the IEEE AP-S Tokyo chapter young engineer award in 1994. He is a Fellow of IEICE and a Senior member of IEEE. He can be contacted at email: omei@faculty.chiba-u.jp.